Deformation of the brick mortar interface in compression and the use of ESPI

A.T. Vermeltfoort
Eindhoven University of Technology, Faculty of Architecture, Building and Planning,
Department of Structural masonry design.

For masonry loaded in compression, the interaction between brick and mortar is of main interest. Tests showed that the deformation-properties of the mortar itself could be measured with ESPI. With the usual measuring techniques this turns out to be difficult as only small gauge lengths are applicable. This paper discusses the ESPI measuring technique and shows some of the effects of joint imperfections on the behaviour of masonry loaded in compression. Precise quantitative information about the deformation of brick and mortar separately was obtained. It may be concluded that the load is mainly transmitted through the central 60 to 70 mm of the specimen. ESPI measurements under various stages of testing confirm the linear behaviour of the specimen up to 80% of failure load.
The bottom load platen of the used moving seating arrangement had too much freedom of movement in relation to the bending stiffness of the specimen around the weak axes and caused unintended deformations.
Lateral deformation could be measured quite simply with ESPI but only provided a general idea of the behaviour of the specimen.

Key words: laser-speckle pattern interferometry, masonry in compression, brick-mortar interface behaviour

1 Introduction

Masonry is used for structures since ages. However, research is still needed, if only because of the development of new materials and their application and new measuring techniques like ESPI. ESPI stands for Electronic Speckle Pattern Interferometry. This laser speckle method allows for contact free deformation measurements with high accuracy.
In masonry where bricks are joined together with mortar, the mortar allows for dimensional tolerances in the bricks, transfers loads and bonds the bricks together. Pointing mortar can improve the esthetical appearance.
One of the main characteristics of masonry is its low tensile capacity. Consequently, well designed masonry structures are mainly loaded in compression and so the interaction between brick and mortar under compressive loads is of main interest. The deformation-properties of the mortar itself are difficult to establish (with the common measuring techniques) as only small gauge lengths are applicable. However, with ESPI new possibilities became available.
The main purpose of this paper is to discus the ESPI measuring technique and to show some of the effects of joint imperfections on the behaviour of masonry loaded in compression. Using ESPI it

was possible to establish the deformation behaviour in compression of mortar and bricks separately. The horizontal deformation of the small specimens was measured as well. The results can be used in numerical research where joint behaviour is modelled in detail. It is an advantage that ESPI results can easily be compared with strain distributions found with numerical simulations.
In the paper first, the brick-laying process i.e. the production of the joint and the contact surfaces with bricks will be discussed, leading to the problems described in this paper; subsequently, the ESPI measuring technique will be explained in chapter 3, section 1; then, the loading system used together with ESPI to measure deformations in compression, will be discussed; finally, the results of two test series will be presented and discussed.

2 The brick mortar interface

2.1 Brick mortar interaction

Failure of masonry in compression is related to the interaction of the unit and the mortar joint as a result of their different deformation characteristics, see e.g. Hendry [1].
To establish the masonry compressive strength, the brick-mortar interaction model, initially formulated by Haller [2] in the late 50ties can be used. In this theory the relationship between strength and stiffness of both mortar and brick was recognised. Based on elastic analysis it is assumed that the mortar expands more in lateral direction, i.e. perpendicular to the loading direction, than the brick. Consequently, tensile stresses develop in the brick. This theory is based on the observation that the (traditional) mortar is much softer than the brick. The stiffness and strength of modern mortars however may be of the same order of magnitude as that of the brick.
After Haller [2], the theory was improved several times [1] and [3] and non linear theories were developed in which the behaviour of unit and joint materials under the action of bi- or tri-axial stresses were incorporated. However, in none of the theories, the effect of joint imperfections is taken into account while material properties are assumed to be homogeneous over the volume of brick and mortar. Anyway, knowledge of mortar deformation behaviour in the wall itself is needed, e.g. for detailed numerical studies. Establishing mechanical properties for mortar in a wall is even more difficult than for brick due to the small gauge length that can be applied as the joint thickness is only 10 to 15 mm. The brick-mortar interaction makes it impossible to measure the 'pure' mortar strength. Usually, the strength of mortar prisms is established with prisms that hardened in steel moulds. The results are used to characterise the mortar but are not representative for the mortar properties in a wall. Therefore, mortar strength is sometimes established by means of cylinders or prisms cut from mortar discs that hardened between bricks [4] and [5].
To obtain a reliable modulus of elasticity of mortar, measurements on masonry specimens are required. Then, E-values for mortar are often established as a subtraction of masonry deformation, Δl_{ma}, and brick deformation, Δl_{br}. The difference, Δl_{mo}, is supposed to be the deformation of the mortar. Based on compatibility, equilibrium and linear elastic behaviour and with equal Poisson's ratios for brick and mortar, the following formula, with t for thickness of a layer, can be derived [3]:

$$\Delta l_{mo} = \Delta l_{ma} - \Delta l_{br} \quad (1a)$$

or:

$$t_{mo}/E_{mo} = (t_{br} + t_{mo})/E_{ma} - t_{br}/E_{br} \quad (1b)$$

with:

Δl	=	length reduction over the gauge length
t	=	thickness
E	=	modulus of elasticity

indices:

mo	=	mortar
br	=	brick
ma	=	masonry

However, effects of joint imperfections are not included in formulae (1a) and (1b), neither the effects due to unequal Poisson's ratios. In these formulae imperfections and flaws are smeared out over the volume. Consequently, these properties remain unknown. Fortunately, the use of ESPI enables measurements of deformations both parallel and perpendicular to the loading direction. Some of the reasons that cause joint imperfections will be discussed in the following section.

2.2 *Joint imperfections caused by brick laying*

The brick laying process is one of the main reasons that material properties are not uniform across the joints. In the Netherlands, the mason puts the amount of mortar required for one brick on the wall. Then, a brick is squeezed into the fresh mortar, and some of the mortar is scraped against the head of the previous brick with the brick being placed. Figure 1a shows what can go wrong during this activity due to bad workmanship. Figure 1b shows the mason seen from the cavity ('dirty') side of the wall. The surplus of mortar is scraped away and thrown back into the container. Trained masons take exactly the required amount of mortar on their trowels and throw almost nothing back. Still they perform well, with completely filled joints. At the visual external side, the joints are raked, approximately 15 mm deep, and later refilled with a pointing mortar. Cord guiding, visible in Figure 1b is used to allow for a smooth and plumb wall.

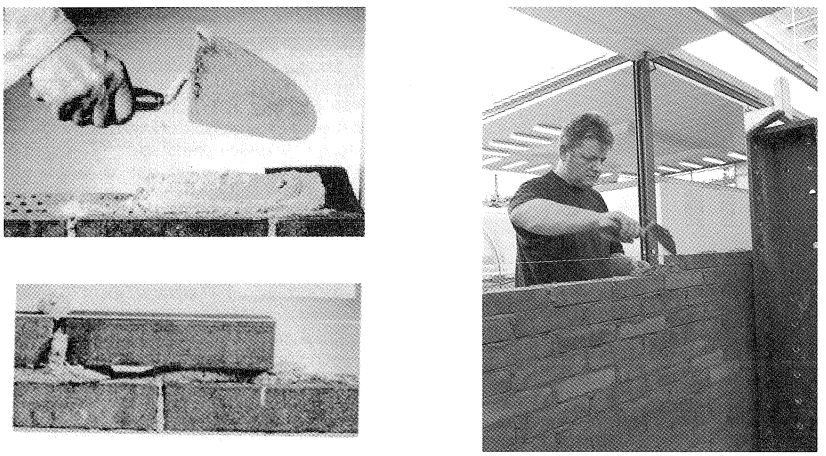

Figure 1: a) Example of a poorly filled joint (left). The brick was squeezed into the fresh mortar but too much of the mortar was scraped against the head of the previous brick with the brick being placed. b) Laying bricks seen from the back side of the wall (right).

In the middle, the mortar is compressed during brick laying and consequently, the edges and header joints are not always completely filled. This 'rounding of the bed joint', is caused during brick laying when a wall is slightly moved in its thickness direction, see e.g. Haller [2] and Sabha et.al. [6]. Setting and early shrinkage of the fresh mortar at the edges makes this effect inevitable.
For good brick laying, the moisture content of the bricks and the workability of the mortar are main parameters. As water absorption from the mortar by the units depends largely on the absorption characteristics of these units, large moisture variation in the transition between mortar and brick can occur, Groot [7]; this also has its effects on the variation of the material properties, especially of the mortar. Sanding of bricks may cause poor bond because the sand works as a kind of insulation. The grains of sand can be well bonded by the mortar but often they are only poorly connected to the brick. The layer of sand will influence the behaviour of the brick mortar interface.
In a nutshell, variation of properties over the width of the joint is caused by 'rounding of the bed joint' while water absorption and brick-sanding will cause variation of the properties over the height of the mortar joint. Examples of joint imperfections due to the brick laying process were found in bond wrench and tensile tests. In the example of Figure 2 only the central area of the bed joint had been bonded. Two other areas can be recognised: an outer area with no bond at all, and a middle area that shrank loose.
Figure 3 shows a photo taken under UV light of section A in Figure 2 perpendicular to the bed joint. The specimen was impregnated with epoxy resin and a material that reacted to UV light. Horizontal openings ('cracks'), even before testing, are clearly visible.
As material properties are not uniform across the joint, this will have its effects on brick mortar interaction and strain distribution. The observed three bond areas in the brick mortar interface cause the (compressive) load to be transferred mainly trough the central area while the stresses at the edges are expected to remain low.

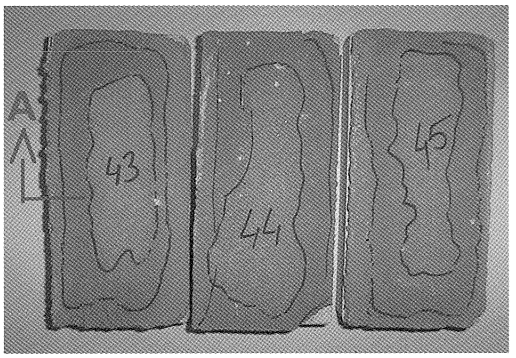

Figure 2: Examples of the top view of three bond areas after bond wrench testing.

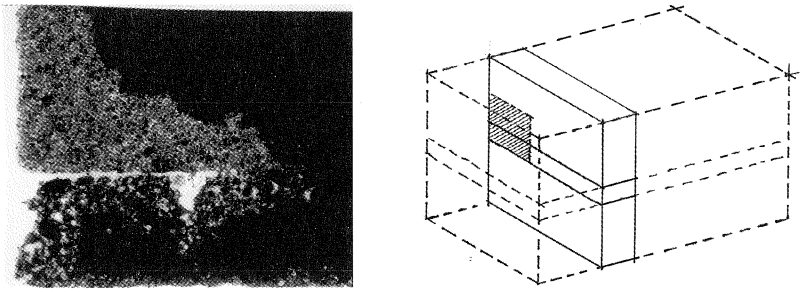

Figure 3: Photo under UV-light of the hatched area in the isometric scheme, (right) showing the outside edge with opening of a unit-mortar interface. Section A in Figure 2.

3 The use of ESPI

3.1 The ESPI system and how it operates

ESPI (Electronic Speckle Pattern Interferometry) is a non-contact 3-D displacement measurement system. The great advantage of a non-contact system like ESPI over contact systems like LVDT's or demec is that it enables the continuous analysis of surface behaviour with great accuracy [8] and [9]. Speckle pattern techniques are not new, but the introduction of computer-image analysis-software made a practical use possible.

The speckle interferometry technique uses the interference characteristics of electromagnetic waves. It is based on the principle that an optically rough surface appears granulated when it is lit by two coherent light (laser) beams from two different positions. This phenomenon is called a speckle pattern and each individual grain is termed a speckle.

In the ESPI instrument, presented in Figure 4, the two coherent light beams are produced by splitting the light beam of one laser diode. Then the two light beams are directed via mirrors. The reflected light is captured with a CCD camera and the speckle pattern that is found, Figure 5 can be stored in a computer. Speckle patterns include the reflection information of each point of the measured object.

During a test, speckle patterns are taken at various load levels. By subtracting speckle patterns taken at e.g. load L1 and load L2, interference fringes are formed, Figure 6. The number of fringes and their widths are a measure for the displacements of the illuminated area.

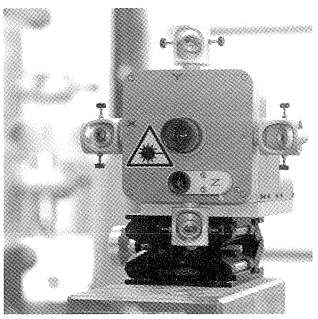

Figure 4: Front of the ESPI apparatus

Thus the displacements of a large number of points, caused by a load increment (e.g. L2 - L1), were measured in a contactless way. Surfaces up to 120 * 120 mm^2 were observed. However, (much) larger areas are possible; however, with a decreased sensitivity.

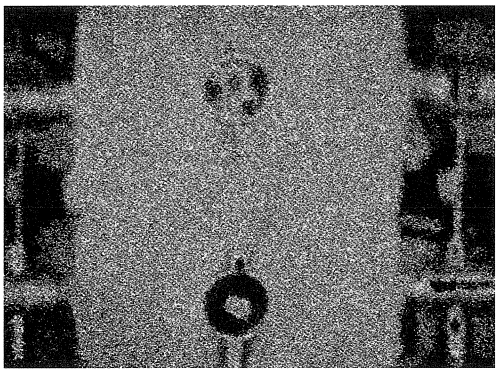

Figure 5: Step 1 in the ESPI process: a speckle pattern is obtained

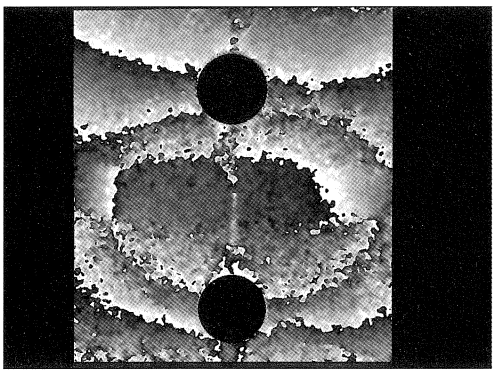

Figure 6: Step 2 in the ESPI process: a fringe pattern is made by subtracting two speckle patterns (the masked circles are caused by the presence of LVDT attachments)

Automatic evaluation of the measurement by real-time subtraction and phase-shifting algorithms is possible. From a fringe pattern of 572 by 768 pixels the displacement can be established, however a data reduction to approximately 50 by 70 points was applied in this project. Displacement and strain distributions were determined with a resolution of 10 nm. By changing the polarity of the laser, displacements in X (horizontal) and Y (vertical) direction were obtained. Displacements in out-of-plane (Z direction) can be measured (however this was not done in this project).
In the next step (step 4) the displacements were plotted. As an example, the vertical displacements of specimen RWA1 are plotted versus their X value in Figure 7. In this tests series an LVDT was positioned in the middle of the surface observed with ESPI and consequently no results were available in that area. This explains the white areas in the middle of Figure 7.

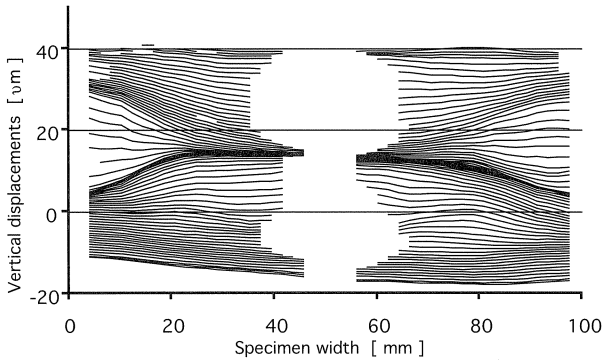

Figure 7: Step 4 in the ESPI process: Vertical displacements of points, plotted versus their horizontal position

At mid height of Figure 7 the distance of the lines that represent the displacements of points in the joint is larger at the edges, from X between 0 and 20 mm and from X between 80 and 100 mm. The lines at the bottom and the top of the figure indicate the brick deformation which is contrary to the joint. For X between 20 and 80 mm the distance between the displacement lines in Figure 7 is more or less equal over the full height.

From the displacements, strains were calculated. However, the load increments at which deformations were obtained were different for each specimen. Therefore, ϵr-values were calculated to facilitate comparison. These ϵr-values represent strains for a stress increase of 1 N/mm^2, in formula:

$$\epsilon r,ij = (vi-vj)/(yi-yj)/\Delta\sigma. \quad (2)$$

with:

$$\Delta\sigma = (L1-L2)/(b*d) \quad (3)$$

and:

vi and vj	=	displacements in vertical direction
yi and yj	=	y values of the two 'measuring' points
(yi-yj)	=	gauge length for strain calculation
b*d	=	loaded area

3.2 Conditions for using ESPI

3.2.1 General

Some important conditions for using ESPI are:

- The surface has to be optically rough which is the case for masonry and concrete.
- In masonry, the mortar has another optical reflection than the units. Consequently, non uniform illumination is possible. In this case, a special spray ('paint') has to be used to prepare the specimens.
- The light intensity is a critical aspect too. In some cases there is too much sun light and objects are overexposed. Then, blinding is necessary.
- Loading arrangement and specimen have to be stable. Often, in the beginning of the test, the

specimen itself is not yet fixed between the load platens. Therefore, most of the ESPI measurements were carried out at a load of approximately $^1/_3$ of the estimated failure load. A vibration-free room is preferred. Vibrations generated by the test itself must be damped as much as possible.

- ESPI measures the displacement differences of points of a surface. If the whole body moves it is difficult to determine small displacement differences. A special test set-up with attachment of the ESPI-apparatus to the specimen itself can be a solution, [10].

3.2.2 Sensitivity

Like when using a photo-camera, the distance between camera and subject is of great importance for the image that is obtained. With a larger distance, a larger surface can be observed, however, the sensitivity decreases, the reflection is weaker and the measuring more difficult. The sensitivity of the ESPI system depends on the wave length of the light produced by the laser diode and on the illumination angle of the laser-beams (i.e. the distance d1 between two mirrors), Figure 8.
In formula:

$$\text{sensitivity} = \text{wave length} / (\sin(\alpha) * 2) \quad (4)$$

where the angle

$$\alpha = \arctan(d1/(2*d2)) \quad (5)$$

In this project the following data are applicable:

wavelength = $783 * 10^{-3}$ μm
d1 = spherical mirror distance = 200 mm
d2 = the object distance, ranging from 600 to 800 mm

From these data it follows that the sensitivity ranges from 2.4 μm to 3.2 μm.

Usually, sensitivity in ESPI is referred to as the needed object deformation to produce one additional fringe. Roughly one fringe (produced by a deformation of 2.4 to 3.2 μm) is represented by 256 colours which means that the resolution, that is the minimal deformation to produce a signal that can be measured, is approximately 10 to 13 nm.

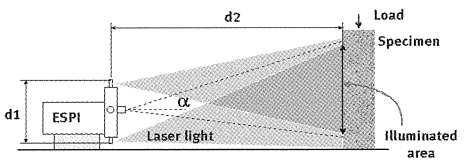

Figure 8: Scheme of the light beams to explain sensitivity

4 The moving seating arrangement

4.1 General description

When a specimen is placed between the loading platens of an ordinary compression machine, the top and bottom of the specimen are restrained to a certain degree in horizontal direction and only the total force can be recorded, without knowledge about its eccentricity.

Because strains found with ESPI were unevenly distributed over the surface, the need was felt to measure forces in more detail. Therefore, a 'moving seating arrangement' was developed and mounted in a Schenk tensile-test machine, Figure 9. In the 'moving seating arrangement' a 70 mm thick steel plate was suspended with three 16 mm steel bars from the upper cross beam of the tensile machine. As shown in Figure 9, the specimen was positioned on this plate. Another 70 mm thick plate above the specimen was mounted with 32 mm thick steel rods down to the bottom of the testing machine. When the cross beam of the machine was moved upwards, the lower plate moved towards the top plate and the specimen was compressed.

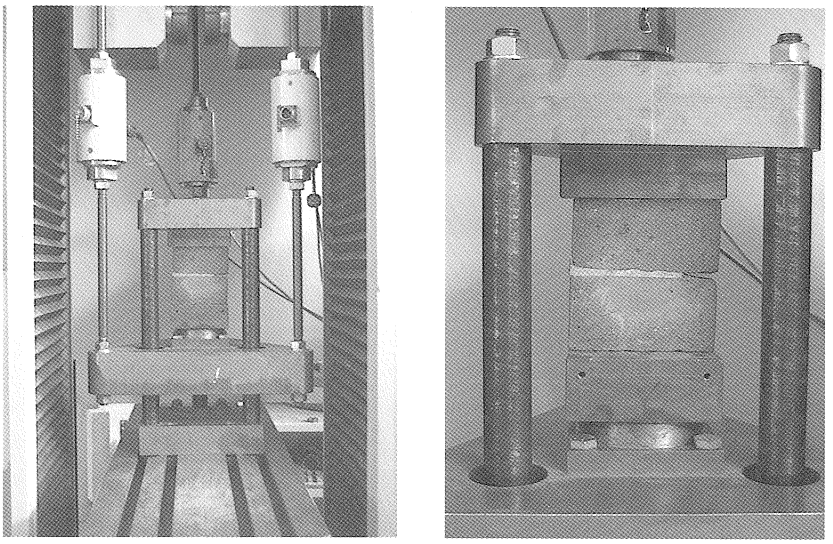

Figure 9: Scheme of the 'moving seating arrangement' and a detail of a specimen in the arrangement. The bending stiffness of the suspension bars with load-cells was considered to be so small that no horizontal forces would develop.

4.2 Load eccentricities

The results of the three load cells and equilibrium of moments was used for the determination of the eccentricities in the load. The bending stiffness of the suspension bars was considered to be so small that no horizontal forces would develop. The effect of the weight of the bottom plate, approximately 400 N, was neglected. Then, the moment of the forces measured by the load cells equals:

$$M = LC1*d1 + LC2*d2 + LC3*d3 \quad (6)$$

and the total load on the specimen equals;

$$N = LC1+LC2+LC3 \quad (7)$$

where:

LC1, LC2 and LC3 = the forces measured by the load cells 1, 2 and 3

d1, d2 and d3 = the distances between the load cells with respect to the centre of the loading arrangement.

With a perfect central loading the moment M would be zero. As an example the moment M is plotted versus N for the specimens JO D2 and RW A2 in Figure 10.

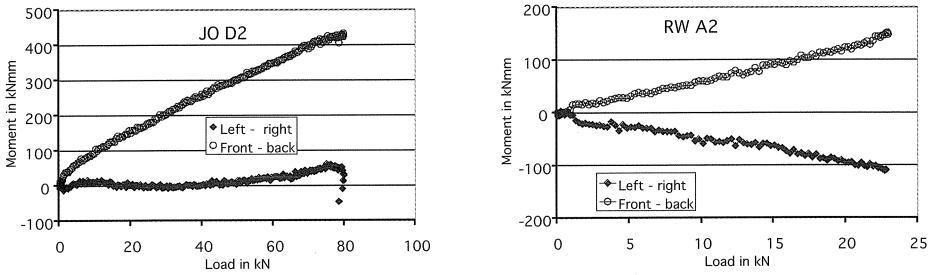

Figure 10: M-N diagrams. After a begin-effect an almost linear relationship can be observed.

For all specimens, the M-N relationship was of the form:

$$M = N\,e + M_0 \tag{8}$$

with:

M = moment of forces in load cells
N = sum of forces in load cells
e = eccentricity of load
M_0 = initial 'setting' moment

Formula 8 shows, that for small values of the load (N) the moment (M) equals M_0. This can be explained as follows. At the start of the test, the opening between the top load platen and the steel block on top of the specimen has to be closed. One point will make the first contact and all (however small) forces have to be transmitted there. Then the eccentricity is less than half the width or half the thickness. Consequently, the specimen is compressed more at the side where the first contact is made. To close the opening, some accelerated rotation, i.e. a moment ($M \approx M_0$) is required and this explains why the M-N graph had a steeper initial curve. This first part of the M-N relationship was neglected when the best fit relationships were established.

The use of M-N relationships rather than e-N relationships is preferred because of the value M_0 in the M-N relationship. For small values of N the value of e would theoretically become infinitive. In the measurements, variation in the small load cell recordings resulted in large variations of the eccentricity which was not practical.

For larger values of N the value of e can be regarded as a constant. Where appropriate, the e value during ESPI recordings will be mentioned.

To allow for the situation that the loaded surfaces of the specimens were not parallel, a ball bearing was used. Specimens were positioned on the ball bearing and rotated manually in order to get the top surface parallel to the top loading plate. By slowly closing the gap between loading plate and specimen and adjusting the position of the specimen at the same time, the load was introduced as evenly as possible.

The load cells could measure a force variation of approximately 12.5 N. This sensitivity of the load cells was sufficient, while it allowed for measurement of moments of minimal 4.15 kNmm and this value was relatively small compared with the measured values. As stated earlier, M-N relation-

ships were almost linear, except in the beginning of a test, and deviations from the best fit line were small. Using best fit methods, the values of M_0 and e could easily be established.

5 Experimental details

5.1 *Materials*

Brick, mortar and masonry properties are presented in Table 1.

Table 1: Brick, mortar and masonry properties.

Brick						Mortar		Masonry
Name	Code	Type	dimension	IRA[1])	f'br [2])	Type[3])	f'mo[4])	f'mas [5])
			mm[3]		MPa		MPa	MPa
Joosten	JO	extrusion	205 x 96 x 50	3	141	MM	22.3	34.7
Rijswaard	RY	soft mud	210 x 99 x 50	44	26	GM	9.6	13.3
						TL	10.1	12.1

[1]) IRA = Initial Rate of absorption gr/dm^2/min

[2]) f'br = brick compressive strength NEN 2489: 1976

[3]) type = MM: medium mortar, GM: general purpose mortar, TL: thin layer mortar

[4]) f'mo = mortar compressive strength, NEN 3850: 1991

[5]) f'mas = compressive strength of a wallette, 50 cm high and 42 cm wide [11], acc. EN1052-1.

5.2 *Specimen dimensions and preparation*

Simultaneously with the small walls (wallettes) described in [11] couplets were made using two bricks with one joint in the middle. The joints were completely filled. From these couplets, all specimens were cut with a water-cooled diamond saw and left to dry before testing. The size of the specimens was approximately 100 mm wide (the width of the brick used), 112 mm high (two times the thickness of a brick and one joint) and 25-27 mm thick. LVDT's were connected in the middle of the left and right hand side of the specimen, Figure 11. Their gauge length was 50 or 65 mm and included the joint. LVDT-results were used for checking the ESPI results. ESPI was used to observe the behaviour of the front surface of the specimen.

Because the ESPI system is based on the reflection of laser light from the surface of the specimen, only surface behaviour can be monitored. However, when a crack or an imperfection is present parallel to the ESPI-observation direction, the deformation of the surface will be small. Therefore, specimens were cut from couplets and the deformation of a cut surface observed. The use of a specimen with two parts of brick and one joint allowed for the study of the behaviour of one joint seperately and a controlled load introduction not distrubed by other joints. The thickness was not too large so not too much confinement occurred because t/h ~ 4 and consequently stresses are assumed to be equally distributed in thickness direction. Only strain variation due to weaknesses of the joint were expected to be observed.

The specimens were capped with a thin layer of gypsum as follows. On a sheet of glass an amount of gypsum was prepared. The glass was oiled in order to prevent the gypsum from sticking to the

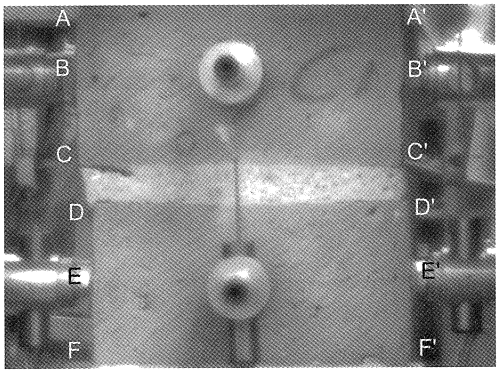

Figure 11: Photo taken via the CCD camera of a specimen with LVDT's. The LVDT in front obstructed the ESPI observations in that area, however, it allowed for a reliable comparison of ESPI and LVDT results. Letters refer to positions for strain calculations, see section 6.1, step 5.

glass. The specimen was pushed into the wet gypsum and placed in vertical position, using steel supporting blocks. After approximately one hour, when the gypsum had hardened, the specimen was taken from the glass sheet by moving it to the side. Subsequently, the process was repeated for the other side of the specimen.

6 Results of mechanical measurements

The strength, stiffness and failure behaviour of the small specimens will be discussed, together with their load eccentricities. These eccentricities were obtained from the three load cell results of the moving seating arrangement as discussed in section 4.2.

6.1 Compressive strength and modulus of elasticity

Averaged compressive strengths and E values of specimens (cut from couplets) and wallettes (from earlier tests [11]) are presented in Table 2. E values were established from LVDT measurements as the secant of the linear part of the σ-ϵ diagram. Therefore, values between approximately 10% and 80% of the failure load were used.

Table 2: Averaged compressive strength and E values

	joint thickness	strength N/mm² Specimen[1])	N/mm² wallette[2])	E value N/mm² specimen[1])	N/mm² wallette[2])
JO	15 mm	46.5	34.7	17300	18400
RY	15 mm	16.3	13.3	4300	4800
RY	3 mm	12.6	12.1	4900	4000

[1]) *specimens, 25 mm in thickness, cut from couplets*

[2]) *wallette results taken from [11]. E value taken at 1/3 of failure load acc. EC 1052-1 specimen: couplet*

The strength of the specimens was considerably higher than wallette strength. Possible causes for strength differences are: a) the number of joints in the specimen, b) the specimen size, c) the type of joint filling, d) weak spots and e) confinement.
Ad a) Only one joint was loaded in the specimens. This is more favourable than the situation for a wallette where load is transmitted from one joint via a brick to another. Irregularities in the transition from brick to joint influence stress transfer in the next joint / brick. Header joints in the wallette make this situation even worse.
Ad b) Specimen size effects estimated as described in [12] showed that differences in strength were not caused by dimension differences because the width to height and thickness to height ratios were approximately the same.
Ad c) There were small differences in the way the specimens were made.
Ad d) It is assumed that larger specimens fail earlier due to the larger number of flaws.
Ad e) There was probably a difference in friction between load platens and specimen surfaces too while the specimens were capped with gypsum and the wallettes with mortar.

Wallettes and specimens, made from the same materials [11], roughly show the same E values. The linearity of the σ-ϵ diagrams was clear from the fact that the R^2 of the linear best fit lines was more than 0.97 in all cases.

6.2 *Failure behaviour*

In general, strong specimens failed much more suddenly than weak specimens. In particular for JO specimens the load displacement diagrams did not give any indication of failure, Figure 12. Fracture of the JO specimens had an explosive character. Pieces were blown away for meters.

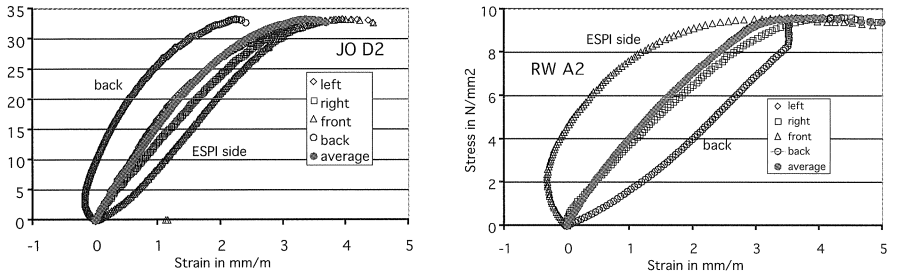

Figure 12: Stress strain diagrams for JO and RY. JO strength was four times RY strength. (Note the different stress scales)

For weaker specimens, failure could be predicted from the load displacement curve. At the end of the test when the specimen has almost failed, LVDT's came loose and were no longer reliable.
In specimens made with JO units the fracture lines in the mortar were under an angle of 70° with the vertical plane in the length of the specimen. Figure 13 shows an example. In the brick an almost vertical cracking pattern occurred. In specimens made with softer RW-bricks the crack ran right through the mortar into the brick. In these specimens shear failure developed. Figure 13 also shows

the unbonded part of the joint that initiated vertical cracking and spalling of the outer 20 mm of the specimen.

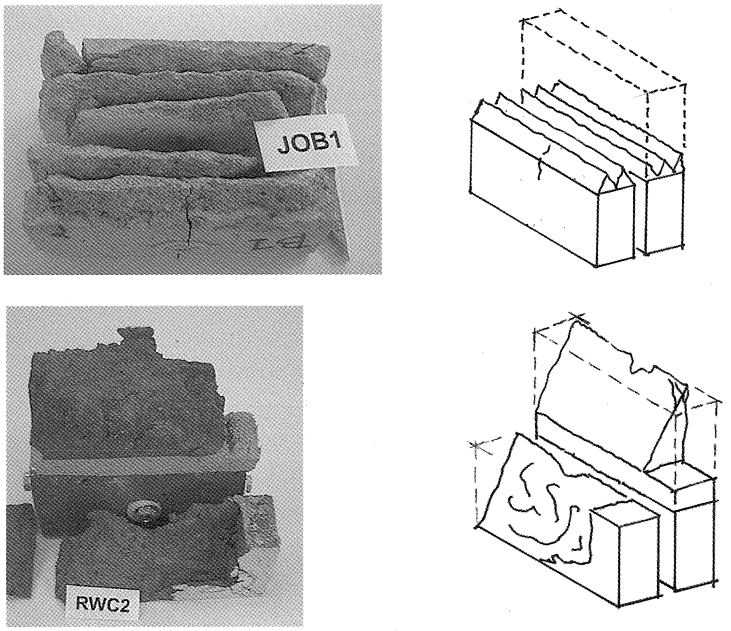

Figure 13: Specimens after testing. Top part put up-side down in front of the bottom part of the specimen. Schematic isometric view and photographs. JOB1 shows the confined mortar, cracked in an angle of approximately 70° as in confined concrete. RWC2 shows the diagonal cracked top brick and the unbonded part of the joint that initiated vertical cracking.

Although, the freedom of movement in thickness direction of the seating arrangement effected the failure mode, the strength of the smaller specimens was higher than wallette-strength [11] as discussed in section 6.1. However, the height (h) over thickness (t) ratio for both specimen and wallettes was approximately four, the larger confinement over the length of the specimens may have had a positive effect on strength compared with the wallettes which had header joints. The failure pattern of the wallettes showed vertical cracks, initiated by the header joints. The specimens often showed diagonal cracks in thickness direction, perhaps due to bending effects as will be discussed in the next section 6.3. An attempt was made to measure the horizontal deformation using ESPI to study the confining effects.

6.3 Variation of load eccentricity during ESPI measurements

Differences in material properties over the width of the specimen caused uneven reactions. Using the forces measured with the three load cells, eccentricities were established from M-N relationships as discussed in section 4.2. In Table 3 eccentricities are given for the loads L1 when the first, and L2 when the second ESPI speckle pattern was taken. To give an impression of the load level at

which ESPI measurements were taken, the estimated maximum load Fmax is given as well. The variation of the load eccentricity during the ESPI measurements was relatively small. The M-N relationship was relatively stable at that stage of the test.
Table 3 shows that the ratios between eccentricity and width (e/w) were considerably smaller than the e/t ratios. The latter refers to eccentricity in the thickness i.e. the ESPI view (Z-) direction while the e/w ratios refer to the eccentricity in the X-direction, that is parallel to the surface observed with ESPI. Bending of the specimen over its weakest axes causes extra tension in the front of one brick and extra compression in the other brick, Figure 14. Consequently, ESPI measured differences in strains for the top and bottom brick.

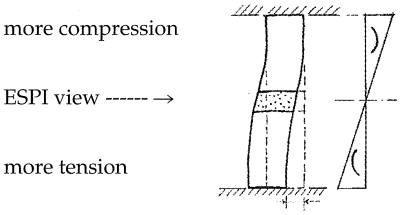

Figure 14: Schematic view of effects of bending around the weak axes

Table 3: Loads (kN) for ESPI measurements and eccentricities (e in mm).

	Load			eccentricities and e/w in width (100 mm) direction for load			eccentricities and e/t in thickness (25 mm) direction for load		
Specimen	L1	L2	F max*)	L1	L2	e/w	L1	L2	e/t
	kN	kN	kN	mm	mm	-	mm	mm	-
RWA1	10	15	35	5.48	5.18	0.05	2.46	1.71	0.07
RWA2	10	13	35	-4.98	-4.60	0.05	6.01	5.80	0.23
RWC1	43	48	35	-1.12	-0.94	0.01	2.29	2.13	0.09
JOB1	43	48	87	6.22	5.43	0.05	6.06	6.40	0.26
JOB2	10	20	87	17.61	12.31	0.12	3.22	2.65	0.11
JOD2	25	35	87	-0.10	-0.13	0.00	7.75	6.69	0.27
JOD3	15	25	87	-1.77	-1.78	0.02	3.18	3.75	0.15

**) estimated failure load, see Table 2. The specimens were not loaded to failure for practical reasons.*

7 Results of laser speckle (ESPI) measurements

First the ESPI results of four tests on JO and three tests on RW specimens (Table 2) will be presented. Then the ESPI results will be compared with the results of LVDT measurements.

For each specimen the ESPI measurements were taken at a certain load level, in most cases approximately around one third of the estimated failure load. Therefore, in the second part of this section,

the strain development during testing of RW specimens both with general purpose (GM) as with thin layer (TL) mortar as observed with ESPI will be treated. Finally, horizontal ESPI-deformations for the three RW and four JO specimens will be presented.

7.1 Results of measurements at one third of failure load

7.1.1 General

As load increments were different for each specimen, εr-values were calculated to facilitate comparison as discussed in section 3.1. For each specimen, εr-values were calculated over the top brick (yi=0 ; yj = 48 mm) over the joint (yi = 48 ; yj = 68) over the bottom brick (yi = 68 ; yj = 105) and over the same length as the LVDT measurements (yi = 25 ; yj = 85). These positions correspond with the

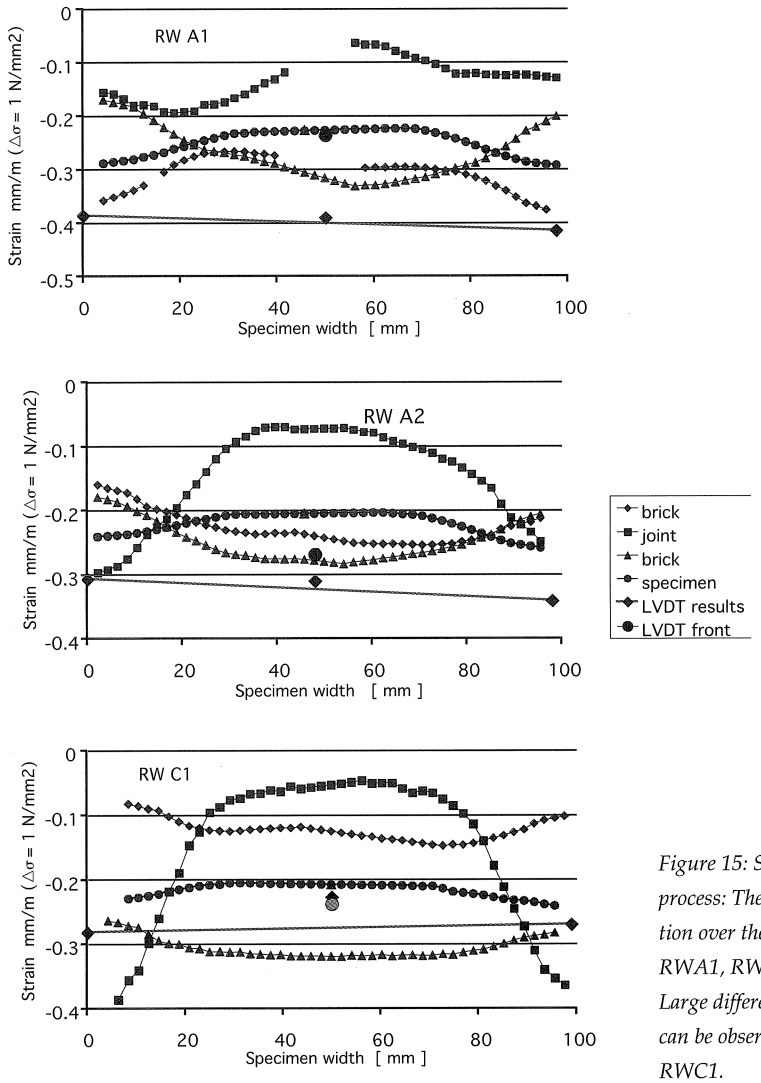

Figure 15: Step 5 in the ESPI process: The εr value distribution over the width of specimens RWA1, RWA2 and RWC1. Large differences in brick-strain can be observed in specimen RWC1.

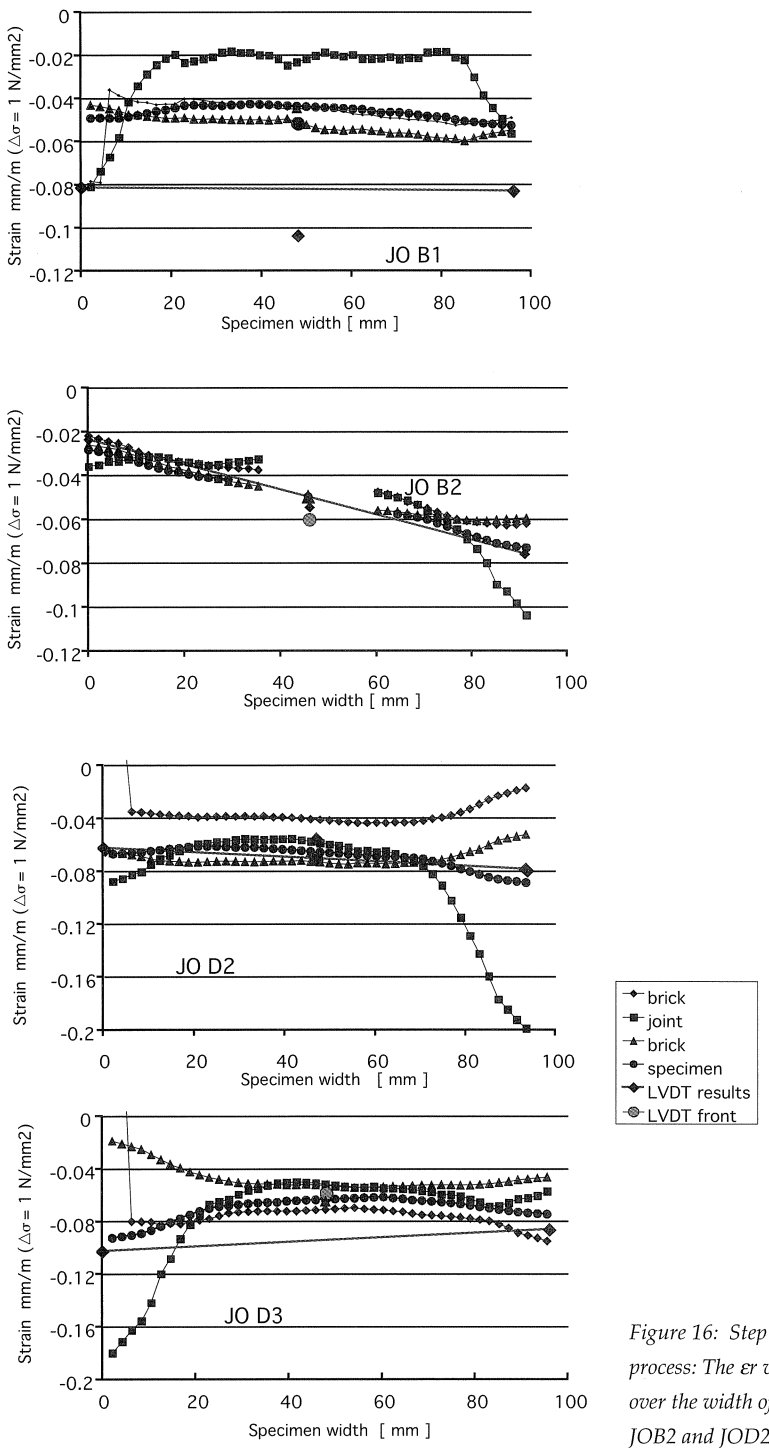

Figure 16: Step 5 in the ESPI process: The εr value distribution over the width of specimens JOB1, JOB2 and JOD2 , JOD3 .

position of lines AA' through FF' in Figure 11. Naturally, εr-values could not be established in the area where LVDT's were present. Where necessary, E-values were calculated by averaging the εr-values over the width of the specimen and calculating $E = 1/\epsilon r$.
The εr-values were plotted versus the width of the specimen, e.g. Figure 15 and Figure 16.

7.1.2 Distribution of er-values over the width

From the εr-value distribution in Figure 15 and Figure 16 it can be concluded that mortar deformations were more extreme than brick deformations. At the edges of the observed surface, the difference between the displacement lines (Figure 7) was the largest. Large mortar strains (εr-values) and small brick strains both indicate small stresses as a consequence of soft spots or cracks. Over the full height of the specimen, the sum of the strains was related to the imposed displacement of the load platens. It may be concluded that at the edges the bricks hardly deform and that the joint together with the interface deforms much more than in the middle.
For the stronger JO specimens, brick and mortar deformed in the same order of magnitude in the middle of the specimen. For RW specimens they differed over the full width.
In the middle of the observed surface, some ESPI results were lacking because the LVDTs were mounted in that area. A linear interpolation was used to compensate the missing ESPI results. Therefore the middle parts of the curves are linear.

7.1.3 ESPI results compared with LVDT results

One of the goals of the tests a was to investigate the compatibility of ESPI and LVDT measurements. Therefore, measurements both with ESPI and LVDT's at one surface were carried out in order to allow for a good comparison between the results.
For a comparison with ESPI, the LVDT results were added in the εr-graphs. In Figure 15 and Figure 16 the εr-values obtained with the left and right LVDT are presented by ◆ shaped dots and connected by a straight line. This line gives an indication of the rotation around the stiff axes of the specimen. Results of the LVDT's on front and back were represented by a ◆ and a ● marker. Their distance is an indication for the rotation around the weak axes of the specimen. The ● marker is the εr-value that was obtained from LVDT-measurements at the ESPI side (front) of the specimen from the centre of the top brick to the centre of the bottom brick. This εr-value is on the line that represents the strain-distribution as measured between lines BB' and EE' in Figure 11. Ideally, the ● marker should be on the straight line between left and right LVDT. The ▲ marker is the result of the interpolation of the ESPI results. The distance between the ● and the ▲ markers is an indication of the difference between ESPI and LVDT results.
LVDT measurements also confirmed the directions of the eccentricities obtained from the forces measured with the three load-cells, Table 3. Table 4 shows the εr-values that were established with LVDT's and ESPI. The er-values of the LVDT results were calculated for the same load increment (from L1 to L2 given in Table 3) as used for the ESPI measurements. The ratio ESPI/LVDT varied between 0.76 tot 1.10. In thickness direction, i.e. in the ESPI view direction, the eccentricity effects are larger as already noticed in section 6.3, see also e.g. Figure 12.

7.1.4 Joint and brick behaviour

As strains for the joints varied most significantly, these strains were isolated for similar specimens from the ϵr-figures in Figure 15 and Figure 16 and collected in Figure 17 and Figure 18. As stated earlier in section 7.1.2, the strains at the edges are larger for the joint and smaller for the bricks than the averaged strains. Stresses were clearly transmitted through the central 60 to 70 mm of the specimen, as assumed earlier. Edge effects, probably caused by mortar shrinkage and rounding of the bed joint can be observed. RW-brick deformations were much more evenly distributed over the specimen width than joint deformation as can be seen in Figure 18.

Table 4: Strains (ϵr-values) in mm/m for LVDT and ESPI measurements and $\Delta\sigma$ = 1 N/mm²

Specimen	LVDT				average	ESPI	ratio
	left	right	front	back	of 4 LVDT's	front	ESPI/LVDT
			A			B	*)
RWA1	0.386	0.414	0.235	0.390	0.356	0.2256	0.96
RWA2	0.307	0.341	0.268	0.310	0.306	0.2038	0.76
JOB1	0.081	0.083	0.052	0.104	0.080	0.0443	0.86
JOB2	0.024	0.076	0.060	0.054	0.053	0.0500	0.82
RWC1	0.281	0.269	0.238	0.227	0.254	0.2065	0.87
RWC2	0.333	0.252	0.185	0.281	0.263		
JO D2	0.062	0.079	0.071	0.056	0.067	0.0653	0.92
JOD3	0.103	0.086	0.058	0.062	0.077	0.0643	1.10

**) Values column A divided by values from column B*

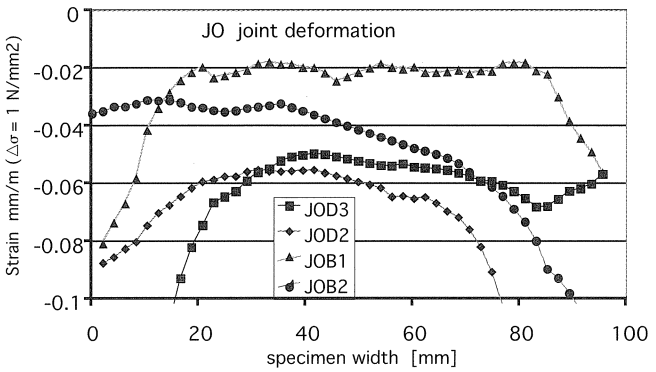

Figure 17: Result for er-value distribution from vertical deformations of the joints for Joosten specimens.

For the JO specimens, see Figure 16, it is clear that the averaged E value of the bedding mortar must be of the same order of magnitude as the E value of the JO units while the measured strains are of the same order of magnitude. Roughly, the E value was 16,500 N/mm² (ϵr-value 0.06 * 10^{-3} mm²/N).

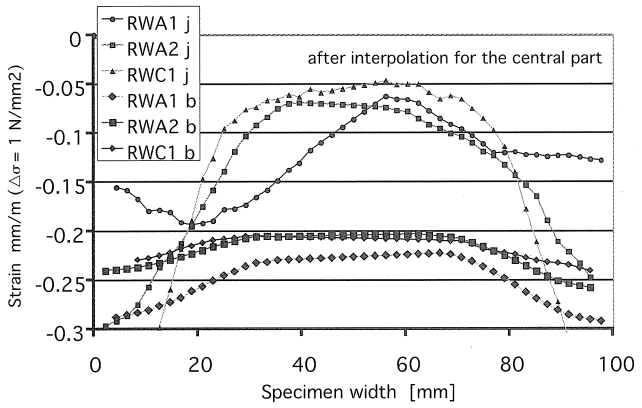

Figure 18: Result for εr-value distribution from vertical deformation in the joints (j) and brick (b) for Rijswaard specimens

Strains for the top and bottom brick showed sometimes a considerable difference, maybe as a result of bending effects as discussed earlier in section 6.3.

In Figure 18 also the averaged top and bottom brick deformations are plotted. Roughly, the RW brick strain (εr) was 0.2 * 10^{-3} mm/m that means E_{brick} = 5000 N/mm^2. and the mortar strain was 0.075* 10^{-3} mm/m or E_{mortar} = 13000 N/mm^2. The E value of the brick almost equalled the value in Table 1 that was obtained from tests on separate bricks.

7.2 ESPI results obtained at various load levels

Another important aspect is the development of strains and strain distribution during a test. In most cases like the specimens discussed in section 7.1, ESPI measurements were made at approximately one third of the estimated failure load. In a separate test series however, measurements were made in all stages of the test to monitor strain development. For these tests, specimens made with RW brick and general purpose or thin layer mortar were used. The same procedure for determining εr-values was followed as in section 3.1. In Figure 19 and Figure 20 joint εr-values are plotted versus specimen width for the RW specimens with thin layer (3 mm joint thickness) and general purpose mortar (12 mm joint thickness). The load levels at which the ESPI-measurements were taken, can be derived from the stress-strain diagrams of Figure 19 and Figure 20.

Comparable tendencies are found for the strain distribution of higher stress levels as was the case in the series of three RW and four JO specimens discussed earlier in section 7.1. However, the magnitude of the strain variation over the width especially for RWTL is larger as the thin-layer specimens show an opening at joint height as can be seen in Figure 9. The effect of this opening at joint height can be seen in Figure 20 where the largest εr-values were found at the open edge at the right hand side (X = 80 – 100 mm).

The εr-value distributions both for small and large loads differed most from the εr-distributions for the loads in between. See e.g. the line for loadstep 4-6 in Figure 19 which deviates from the lines from the other load-steps. At small loads, instability effects of the moving seating arrangement are large, see e.g. Figure 12 and Figure 10. When failure loads were almost reached, instability effects developed in the ESPI results while the specimen started to crack and consequently, stress distribution through the specimens changed. This also could be concluded from the variations in the M-N diagrams of e.g. Figure 10 and the σ-ε diagram of e.g. Figure 12.

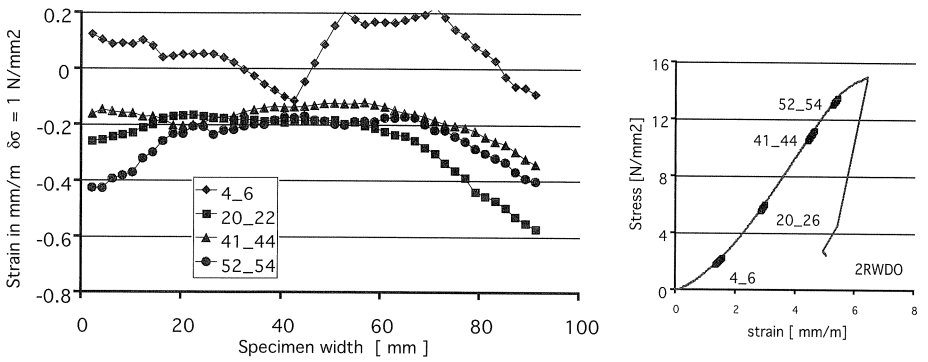

Figure 19: for various load steps, right. Specimen RWDO 2

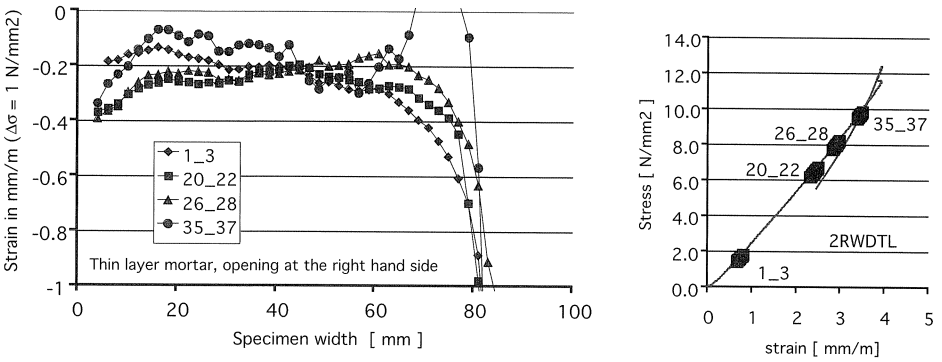

Figure 20: Strains (εr) for joints (left) for various load steps, (right). Specimen RWDTL 2

7.3 *Horizontal displacements at one third of failure load*

When the behaviour of brick and mortar is modelled in detail, cooperation of brick and mortar is often assumed e.g. Haller [2]. Due to differences in Poisson's ratios, lateral expansion of brick and mortar cause lateral tension in the brick and consequently failure. However, lateral expansions are difficult to determine from ordinary walls with LVDT or demec but more insight in their magnitude is necessary to model masonry failure. Therefore, ESPI was used to measure the *horizontal deformation* of the specimens in the same way as the already discussed vertical deformations. The data were handled in the same manner as the vertical deformations, as mentioned in sections 3.1 and 7.1. The horizontal displacements of the grid points were plotted versus the Y values of these points and the results of points with the same X values were connected with straight lines. Figure 21 shows an example.

In most cases it was observed that the top brick rotated while the deformation of the bottom brick was more or less symmetric around the vertical axes, and the deformation of the top brick was more symmetric around an inclined line. Rotation of the top brick was already found when the vertical deformations were studied, e.g. for specimen JO B2, Figure 16.

The deformations of the bricks show a barrel shape as an effect of the confinement by the load platens and the joint, and the uneven load transfer in the centre of the specimen.

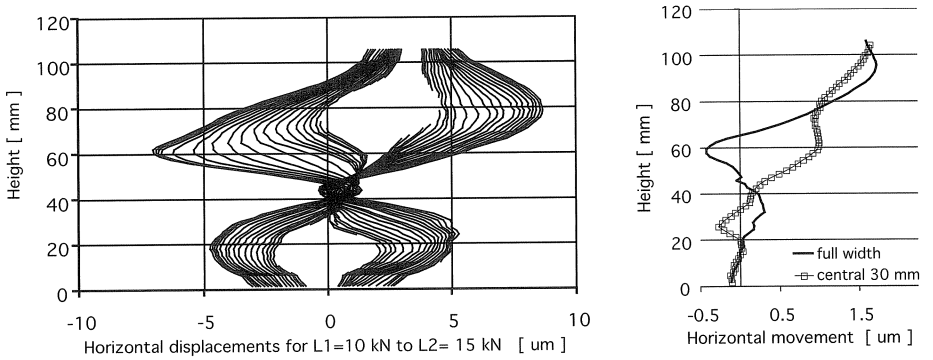

Figure 21: Horizontal displacements (left) show a barrel shape (RWA1). White areas beacause of the obstruction of the ESPI view by the LVDT. Displacement of centre part of the specimen (right).

The ϵr-values (strains for a stress difference $\Delta\sigma = 1$ N/mm^2) in lateral direction were determined by dividing the difference of displacements of the edges by the width of the specimen. Locally, strains will be much more irregular as can be concluded from the distance between the displacement lines in e.g. Figure 21. In Figure 22 horizontal strains (ϵr-values) are plotted for the four JO and three RW specimens, respectively.

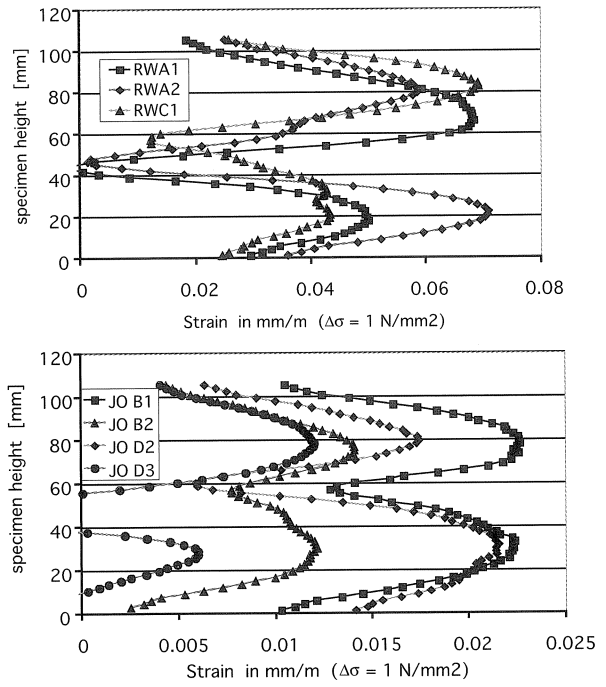

Figure 22: Horizontal strains (ϵr-values) over the height, RW specimens and JO specimens

Smaller εr-values were found at a height between 50 and 60 mm were the joint is situated. Probably, εr-values were smaller because the edges had smaller stresses than the central area. To verify this, for these tests also the strain distribution over the height was calculated for an area of 30 mm width in the centre of the observed area. It turned out that shape and distribution of strains over the full width of the specimen and those over the 30 mm area were more or less equal and consequently an influence of stress differences between the outer and the central area could not be established. The εr-values of the loaded top and bottom edges of the specimen were of the same order of magnitude as those of the joints indicating the confinement by the load platen at the gypsum capping was of the same order of magnitude as the confinement by the joint.

8 Discussion

The use of ESPI to study seperately the behaviour of one joint, required the use of relatively thin specimens cut from couplets. It was assumed that stresses near the joint in the relatively slender (h/t = 4) specimens were not effected by the load platen confinement effect. Further, the cut surface can be observed with ESPI and represents a cross section of a wall.
The ESPI system provided detailed information for each separate specimen. The behaviour of each individual specimen can be monitored accurately. The comparison of results of several specimens is difficult as each specimen behaved differently as the eccentricity deviated considerably from specimen to specimen
A comparison of strength and stiffness of these smaller specimens with those of wallettes showed that specimen strength was in average 1.49 times the strength of wallettes made with the same materials at the same time and from the same mortar batches. E values were almost equal. The main reason is probably that the specimen only has one joint, compared to the five joints in the wallette, so the volume ratio between brick and mortar in the specimen was larger than in the wallette. Probably, horizontal confinement in the specimens had more effect on strength than horizontal confinement in the wallets. However, the height over thickness ratios were the same. Horizontal deformation as observed with ESPI showed a similar lateral deformation at joint height as at load platen height (Figure 22) indicating that the confinement by the load platen was of the same order of magnitude as the confinement by the joint.
The moving seating arrangement was used to allow for a better understanding of the load distribution trough the specimen. ESPI measurements showed unequally distributed strains and necessitated to measure not only the load in the machine but also its eccentricity. The tensile bars that carried the bottom load platen were flexible and allowed for almost free horizontal movement of the load platen. However, the freedom of movement in the ESPI view direction caused bending around the weak axes (Figure 14) of the specimen and consequently stress variation in the observed surface, e.g. Figure 15.
Load eccentricity has a significant effect on the strain distribution. The eccentricity in thickness direction was larger than expected and blurred the results. Consequently, the positioning of the moving seating arrangement in the machine asks for extra attention. An extra complication is that the centre of the loaded area does not necessarily coincide with the centre line of gravity in the specimen due to flaws in units and mortar.

The boundary conditions and the method of load introduction need extra attention as only the surface of a specimen can be observed. Stress and strain at the outside may differ considerably from the expected values based on linear elastic behaviour and $\sigma = N/A \pm M/W$. Horizontal movement of the bottom plate of the moving seating arrangement in the direction parallel to the ESPI-view direction should be prevented, and specimen-thickness increased to reduce bending effects around the weak axes of the specimen.
Eccentricity was obtained from the forces measured by the load cells. When linear elastic behaviour is assumed, it should also be possible to calculate eccentricity from LVDT results. However, measured deformation depended on the position where LVDT's were mounted as indicated by the ESPI deformation measurements. Also the interaction between the specimen and the free moving seating initiated unintended deformation due to bending and, possibly, torsion.
It was difficult to obtain reliable E-values from the ESPI measurements, considering the large variation of the deformations. However, a rough estimation showed that the E-values of the specimens were of the same order of magnitude as those of the wallettes.

9 Conclusions

Using ESPI and the developed experimental techniques it is possible to obtain quantitative information about brick and mortar deformation under compressive loading in a specimen where the same interaction occurred as in a real wall.
The effects of the unbonded mortar interface at the edges are confirmed by the strain distribution over the width of the specimen. From these measurements it may be concluded that load is mainly transmitted through the central 60 to 70 mm of the specimen and that the weak unbonded areas are hardly loaded.
ESPI measurements in various stages of testing confirm the linear behaviour of the specimen from approximately 15 % to 80 % of failure load as measured with LVDT's. The usual non linear behaviour at the start and at the end of the tests can be explained from the interaction between specimen and moving seating arrangement. This interaction caused unintended deformations due to bending and perhaps torsion of the specimen. At the end of testing the interaction between specimen and loading arrangement may have accellerated failure. The bottom load platen had too much freedom of movement in relation to the bending stiffness of the specimen around the weak axes to produce the desired concentric loading in thickness direction.
Lateral deformation could be measured quite simply with ESPI but only provided a general idea of specimen behaviour and joint effects.

Acknowledgement:
The financial support of the Dutch Masonry Foundation is gratefully acknowledged. Participants in the foundation are the clay brick, calcium silicate and concrete units industries and mortar manufacturers.

References

[1] Hendry, A.W., Structural masonry, Macmillen Education Ltd, 1990, pp. 52..65

[2] Haller, P., (Dutch translation 1967) Die technische Eigenschaften von Backstein, Schweizerische Bauzeitung, 1958.

[3] Drysdale, R.G., A.A.Hamid, L.R. Baker, Masonry structures, behaviour and design, Prentice Hall, Englewood Cliffs, New Jersey, 1993, pp. 200.

[4] Vermeltfoort, A.T., Mechanical compressive properties of small sized mortar cylinders, Proc. 8th Can. Mas. Symp. Jasper, 1998, pp. 336..347

[5] NN, Vorläufige Richtlinie zur Ergänzung der Eignungsprüfung von Mauermörtel, Deutsche Geselschaft für Mauerwerksbau e.v. 1992.

[6] Sabha A., Schöne I., Untersuchungen zum Tragverhalten von Mauerwerk aus Elbesandstein, Bautechnik (Ernst & Sohn Verlag) Nr 71, 1994, pp 161-166.

[7] Groot, C., 1993, Effects of water on mortar-brick bond, PhD Thesis, Delft

[8] Newport, Brochure of the ESPI SD-30 system, Newport Instruments AG Giessenstrasse 15, CH-Schlieren, Switserland.

[9] Jones, R., C. Wykes, Holographic and speckle interferometry. Cambridge university press. Cambridge, 1983

[10] Hegger, J.; Görtz, S.; Wijen, E., Analyse der Schubrißbildung unter Einsatz der Laser-Interferometrie, To be published.

[11] Pluijm, R. van der, Korteduur- en langeduurgedrag van baksteen metselwerk, TNO Rapport 1999-con-R3020

[12] Vermeltfoort A.T., Effects of the width and boundary conditions on the mechanical properties of masonry prisms under compression, Proc. 11th Int. Brick/Block Masonry Conference, Shanghai, 1997, pp. 181-190